Supporting Information

The Reduction Behavior of Cubic In_2O_3 Nanoparticles by Combined Multi-*In Situ* Spectroscopy and DFT

Marc Ziemba[1], Leon Schumacher[1], Christian Hess[1*]

[1]Eduard Zintl Institute of Inorganic and Physical Chemistry, Technical University of Darmstadt, Alarich-Weiss-Str. 8, 64287 Darmstadt, Germany

*email: christian.hess@tu-darmstadt.de

Experimental Section

Preparation. In_2O_3 sheets were synthesized by calcining $In(OH)_3$ at 600 °C. For this purpose $In(NO_3)_3{\cdot}xH_2O$ (Alfa Aesar, ≥ 99.99%) was dissolved in deionized water, which was then set to a pH value of 10 using ammonia (ω = 25%). The precipitated $In(OH)_3$ was filtered off and washed five times with deionized water. The residue was dried in an air stream and calcined at 600 °C for 2 h at a heating rate of 10 °C/min. Afterwards the obtained In_2O_3 was sieved using a 200 μm sieve.

Transmission Electron Microscopy (TEM). The transmission electron microscope (JEOL JEM-2100F, Tokyo, Japan) is equipped with a Schottky field emitter and operates at a nominal acceleration voltage of 200 kV. For preparation, the sample was dispersed in an ultrasonic bath for 30 s in ethanol and then placed on a carbon grid (Plano). After drying, the grid was coated with carbon (Bal-Tec MED010) to prevent charging by the electron beam.

Specific Surface Area. N_2 adsorption at 77 K was carried out on a SURFER (Thermo Fisher Scientific). Prior to the measurement, the sample was outgassed at 80 °C in high vacuum (10^{-6} bar) for 48 h. To determine the specific surface area the N_2 adsorption curve was fitted to the Brunauer–Emmett–Teller (BET) model.[1]

X-Ray Diffraction (XRD). Powder XRD patterns were recorded on a Stoe Stadi P diffractometer with a Ge(111)-monochromator, Cu Kα radiation (λ = 1.54060 Å), and a MYTHEN-1K Dectris detector, using a flat sample holder in transmission geometry. The powder XRD patterns were recorded (*ex situ*) after synthesis of the particles and after H_2 treatment for 1 h at 250 °C (10% H_2/Ar, 100 mL/min).

X-Ray Photoelectron Spectroscopy (XPS). XP spectra were recorded on a modified LHS/SPECS EA200 MCD system described previously.[2,3] The XPS system was equipped with a Mg Kα source (1253.6 eV, 168 W), and the calibration of the binding energy scale was performed with Au $4f_{7/2}$ = 84.0 eV and Cu $2p_{3/2}$ = 932.67 eV signals from foil samples. Before measurements, some samples were treated with gas and temperature programs. The subsequent transfer of the sample to the analysis chamber was performed without exposure to air (quasi *in situ*). Sample charging was taken into account by setting the peak of the C 1s signal to 284.8 eV. Survey spectra were recorded at a resolution of 0.4 eV and detail spectra at a resolution of 0.1 eV. The deconvolution of the spectra was performed analogously for all measurements using Gauss–Lorentzian product functions (30/70), whereby the background was subtracted by the Shirley method. All positions change by a maximum of 0.2 eV when comparing all measurements (see Figure 3B), which is within the experimental error. For this reason, it can

be assumed that no metallic indium or indium hydroxide is present on the surface, independent of the pretreatment.

The O:In ratios given in Table S1 were obtained by integrating the In $3d_{5/2}$ signal and the O 1s signal after a Shirley background subtraction from the detailed spectra. The integration boundaries were the same for all measurements. Please note that we attribute the shoulder of the O1s signal at higher binding energies to oxygen atoms near oxygen defects, since hydroxide species are found at slightly higher binding energies.[4,5] For this reason, this area is also included in the calculation of the O:In ratio. The resulting areas were corrected with the corresponding relative sensitivity factors, i.e., 3.9 for the In $3d_{5/2}$, 0.66 for the O 1s, and 0.25 for the C 1s signal.[6] All samples reduced with hydrogen (10% H_2/Ar) were pretreated with O_2 (25% O_2/Ar) at 120 °C. The total flow rate was always 100 mL/min.

***In situ* Raman Spectroscopy (385 nm).** *In situ* Raman spectra with an excitation wavelength of 385 nm were recorded on a Raman spectrometer described previously,[7,8] using a commercial CCR1000 cell (Linkam Scientific Instruments) equipped with a CaF_2 window. The power of the laser at the sample was set to 8.5 mW. Before the measurements, the sample was heated for 1 h at 120 °C at a flow rate of 50 mL/min (25% O_2/He). Afterwards, spectra were obtained in O_2 flow (25%) at 25 °C, in H_2 flow (7%) at 25 °C, and in H_2 flow at 120 °C (total flow rate: 50 mL/min). Spectra were obtained from a sum of two spectra with a measuring time of 20 min each in addition to cosmic ray removal, which results in a total measuring time of 1 h. Raman spectra are presented after background removal.

***In situ* Raman Spectroscopy (532 nm).** Raman spectra were recorded on a HL5R transmission spectrometer (Kaiser Optical), employing a frequency-doubled Nd:YAG laser (Cobolt) for excitation at 532 nm, as described previously.[9,10] The spectral resolution is specified as 5 cm^{-1}, and the stability of the band positions is better than 0.3 cm^{-1}. The laser power at the position of the sample was set to 6 mW. For *in situ* measurements 20–25 mg of sample was placed in a stainless-steel sample holder (diameter: 8 mm; depth: 0.5 mm) and exposed to a gas flow of 25% O_2 /Ar (total flow rate: 100 mL/min). In_2O_3 was measured using an exposure time of 900 s and 2 accumulations. For each measurement a cosmic ray filter was used. As a result, the total measuring time amounted to about 1 h.

***In situ* UV-Vis Spectroscopy.** The UV-Vis spectra were taken in diffuse reflection using an AvaSpec ULS2048 spectrometer (Avantes) equipped with a deuterium lamp and a halogen discharge lamp. The measuring time was 60 s, which is composed of an exposure time of 300 ms and 200 runs. As the white standard, magnesium oxide powder (MgO, Sigma Aldrich) was used, which shows no absorption between 170 nm and 1100 nm. The measurements were

taken under the same conditions as for the Raman measurements (λ_{ex} = 532 nm) before and after each Raman spectrum.

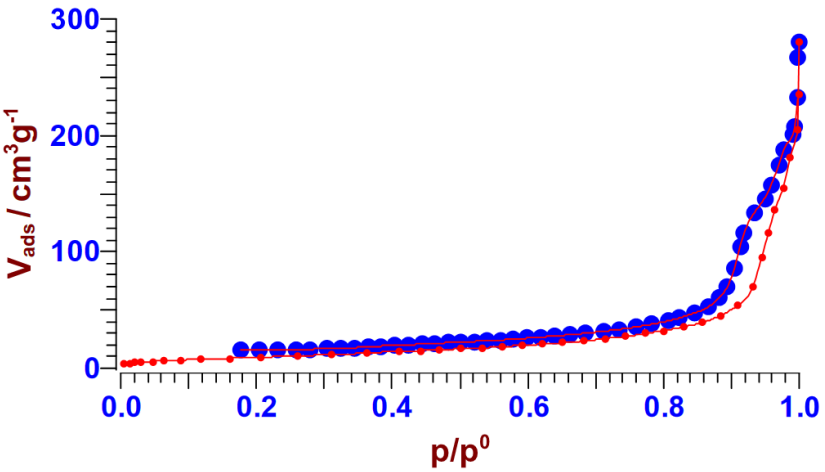

Figure S1: Nitrogen adsorption–desorption isotherm of In_2O_3 nanoparticles.

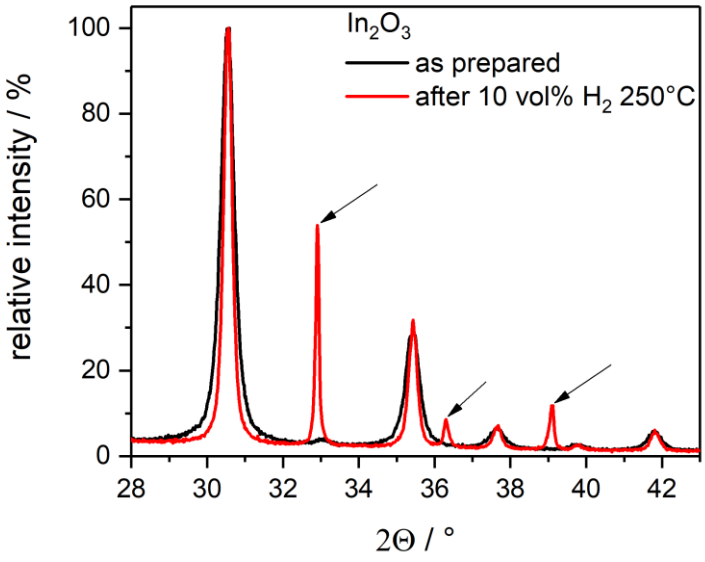

Figure S2: XRD pattern of the In_2O_3 nanoparticles as prepared (black) and after exposure to H_2 at 250 °C (red). The arrows mark the reflections of metallic indium.

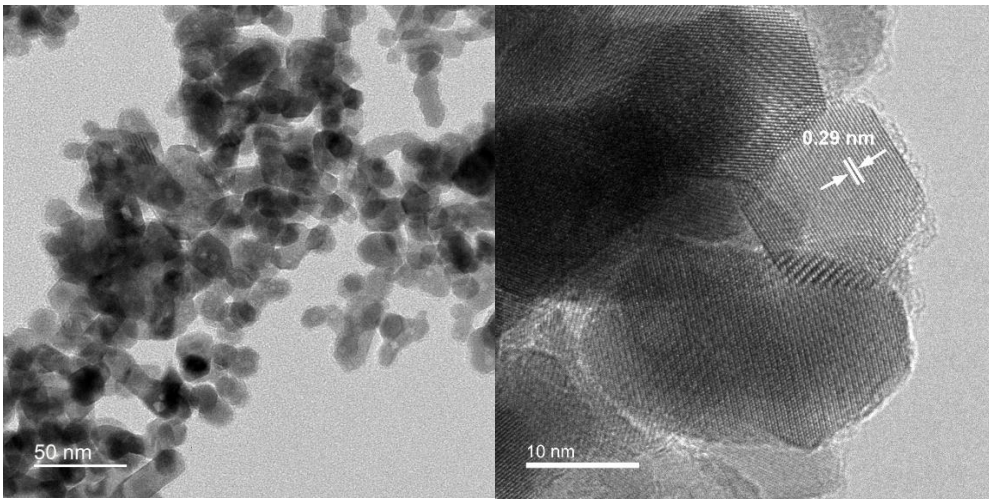

Figure S3: TEM image (left) and detailed TEM image (right) of In_2O_3 nanoparticles. The white arrows indicate the distance between lattice planes in the direction of the particle surface.

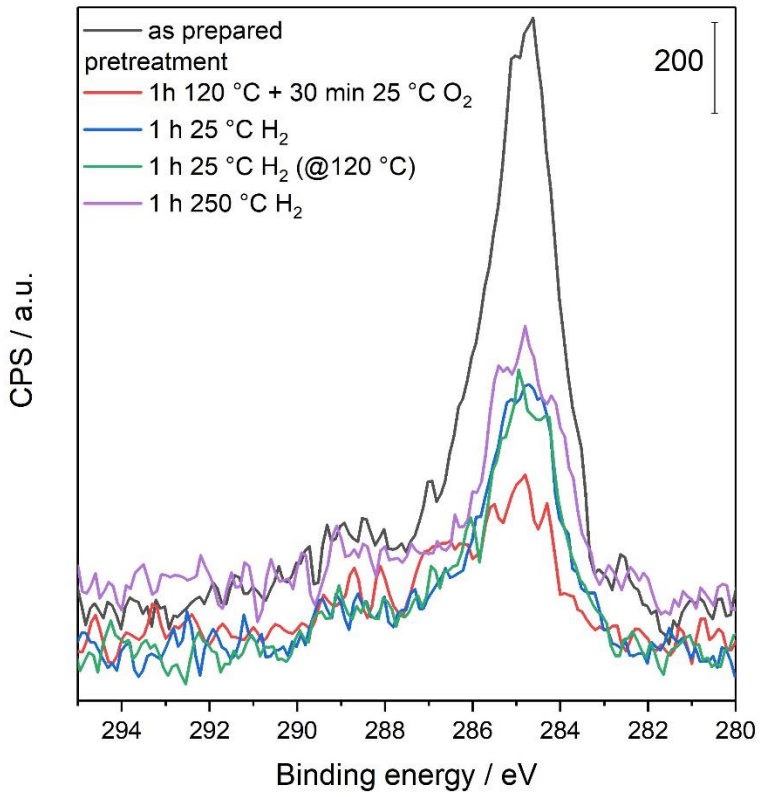

Figure S4: C 1s photoemission of In_2O_3 nanoparticles. The black spectrum was obtained directly after synthesis, the red one after O_2 (25%) pretreatment, the blue and green ones after H_2 (10%) pretreatment at 25 °C, and the violet one after H_2 pretreatment at 250 °C. All spectra were recorded at 25 °C, except for the green one, which was recorded at 120 °C.

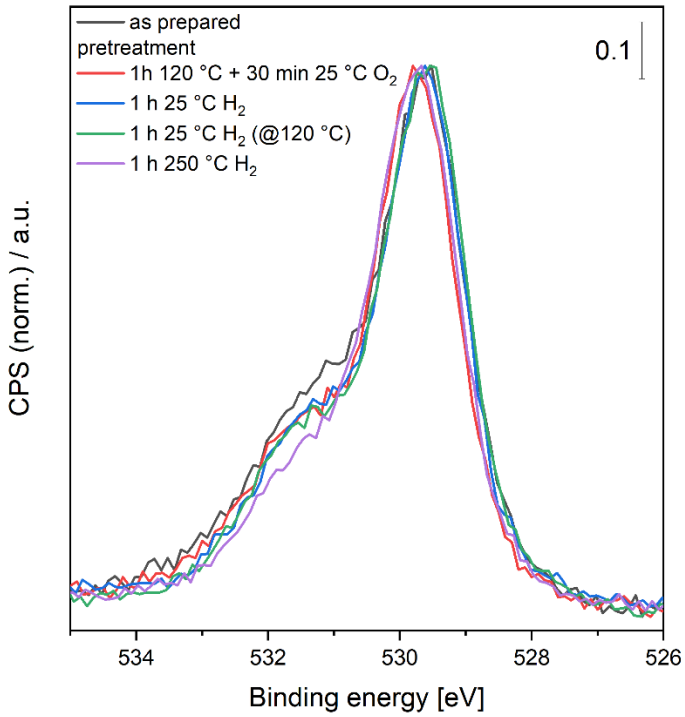

Figure S5: O 1s photoemission of In_2O_3 nanoparticles. For better comparability the spectra were normalized to the highest intensity signal. The black spectrum was obtained directly after synthesis, the red one after O_2 (25%) pretreatment, the blue and green ones after H_2 (10%) pretreatment at 25 °C, and the violet one after H_2 pretreatment at 250 °C. All spectra were recorded at 25 °C, except for the green one, which was recorded at 120 °C.

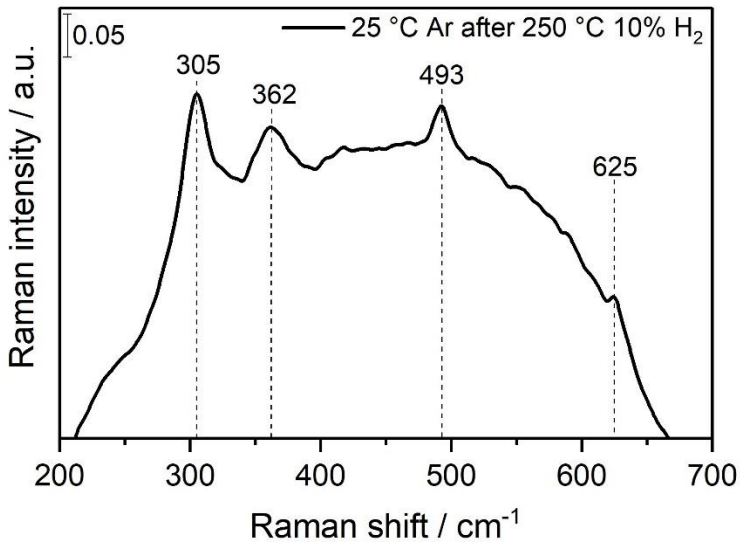

Figure S6: *In situ* 532 nm Raman spectra of In_2O_3 nanoparticles recorded in argon at 25 °C after a 1 h pretreatment in 10 % H_2 at 250 °C.

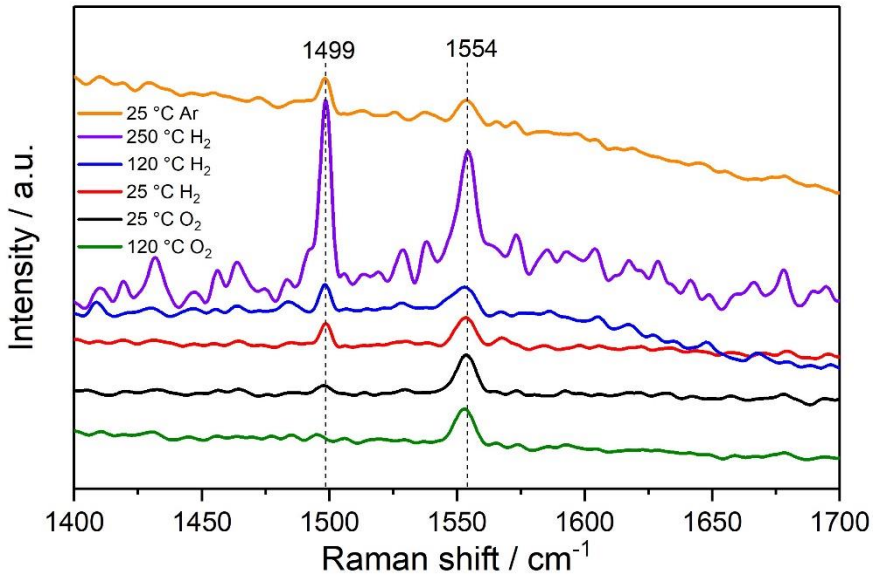

Figure S7: In-H region of *in situ* Raman spectra (λ_{ex} = 532 nm) of In_2O_3 nanoparticles. Spectra were recorded at the indicated temperatures, at a total flow rate of 100 mL/min, and by applying a feed of 25 % O_2/Ar for oxidative and of 10 % H_2/Ar for reductive conditions. Spectra are offset for clarity.

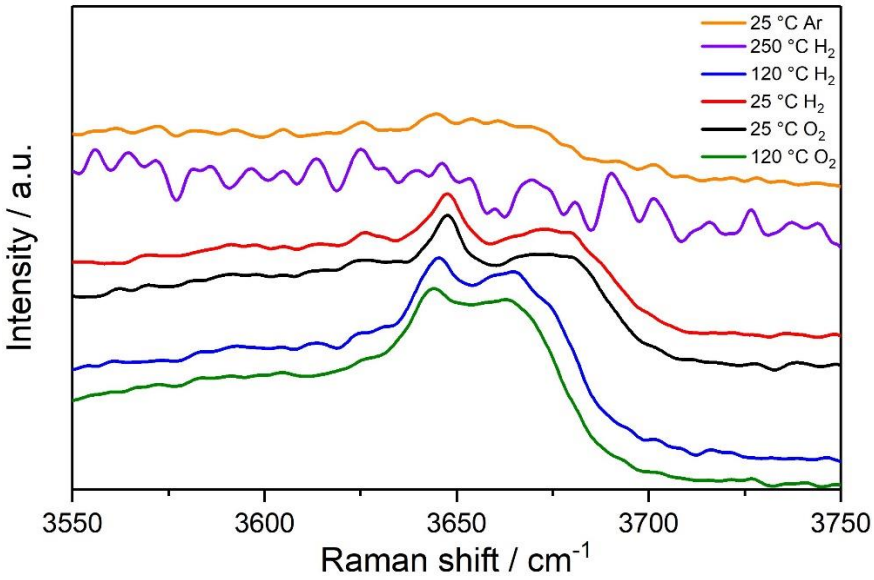

Figure S8: O-H region of *in situ* Raman spectra (λ_{ex} = 532 nm) of In_2O_3 nanoparticles. Spectra were recorded at the indicated temperatures, at a total flow rate of 100 mL/min, and by applying a feed of 25 % O_2/Ar for oxidative and of 10 % H_2/Ar for reductive conditions. Spectra are offset for clarity.

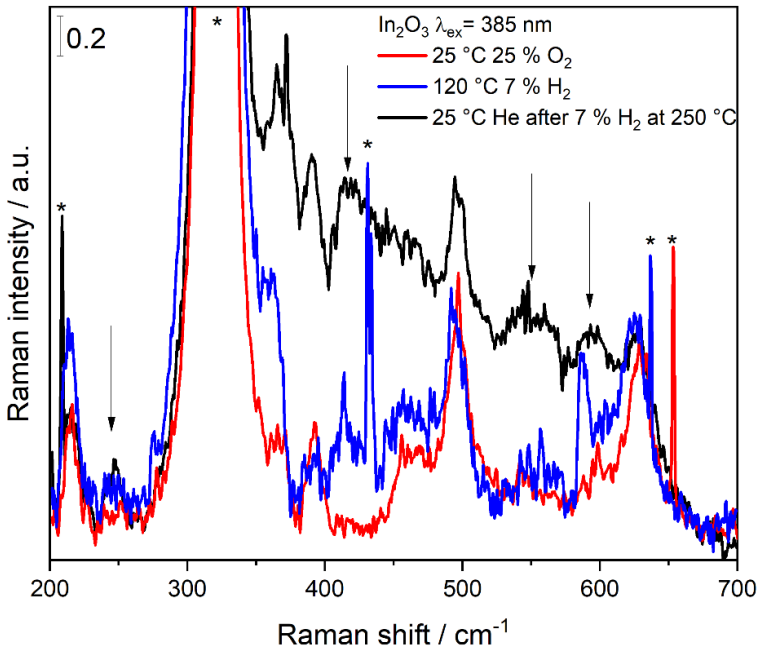

Figure S9: Comparison of *in situ* 385 nm Raman spectra of In_2O_3 nanoparticles recorded at 25 °C in 25% O_2/He (red) and recorded at 120 °C in 7% H_2/He (blue) (pretreatment: 1 h, 120 °C, 25% O_2/He, 50 mL/min). In addition, a spectrum in helium at 25 °C after a 1 h pretreatment in 7 % H_2 at 250 °C is shown (black). The black arrows indicate the defect-related bands. The asterisks (*) mark bands originating from the CaF_2 window, while the sharp features result from cosmic rays.

Table S1: Surface composition (in at.%) and O:In ratios obtained from XPS measurements. Please note that the surface composition was derived from survey spectra and the O:In ratios from detailed spectra. Furthermore, detailed spectra were recorded about 15 min after the survey spectra.

Pretreatment	**C / at.%**	**O / at.%**	**In / at.%**	**O:In ratio**
As prepared	23.0	46.5	30.5	1.47
1 h 120 °C O_2, 30 min 25 °C O_2	5.8	56.0	38.2	1.44
1 h 25 °C H_2	8.1	54.6	37.3	1.36
1 h 25 °C H_2, 120 °C in analysis chamber	8.6	53.3	38.1	1.38
1 h 250 °C H_2	8.2	54.5	37.3	1.40

Computational Section

Density Functional Theory (DFT) Calculations. Calculations were performed using the spin-polarized DFT approach as implemented in the Vienna Ab initio Simulation Package (VASP, Version 5.3.5, https://www.vasp.at/), with the generalized gradient approximation of Perdew, Burke and Ernzerhof (PBE)[11]. The In (4d, 5s, 5p) and O (2 s, 2p) electrons were explicitly treated as valence states within the projector augmented wave (PAW) method[12] with a plane-wave cutoff of 500 eV, whereas the remaining electrons were treated as part of the atomic cores. To calculate the bulk equilibrium lattice constant, several primitive In_2O_3 cells ($Ia\bar{3}$) with different lattice constants were relaxed using a cutoff of 800 eV, and total energies and forces were calculated with a precision of 10^{-8} eV and 10^{-2} eV/Å for electronic and force convergence, respectively. For all additional calculations total energies were calculated with a precision of 10^{-6} eV. This results in a lattice constant of 10.298 Å. The plot of the lattice constant against the total energy is shown in Figure S10. The sampling of the Brillouin zone is realized by (6×6×6) and (3×3×3) Monkhorst–Pack grids[13] for the primitive cell and the unit cell, respectively.

After relaxation, a normal mode analysis was performed followed by a calculation of the Raman intensities using density functional perturbation theory (DFPT). For more detailed information on this approach please refer to our previous studies.[14]

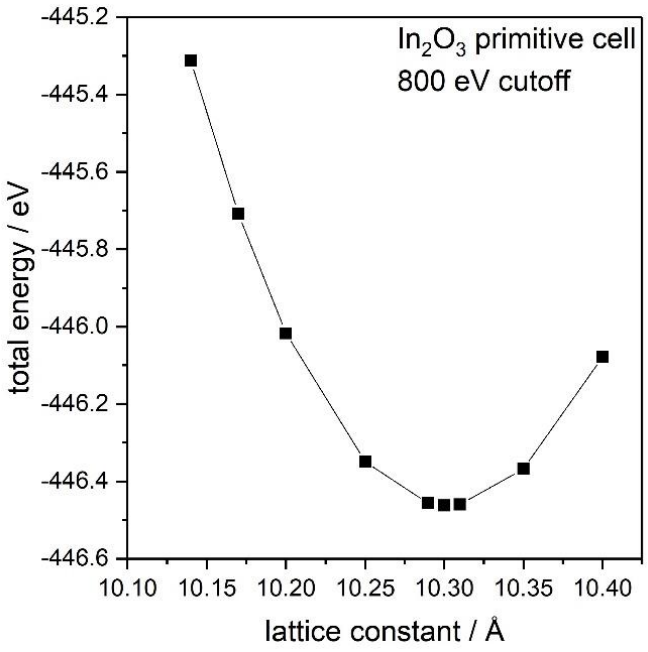

Figure S10: Total energy of primitive In_2O_3 cells ($Ia\bar{3}$) as a function of lattice constant using a cutoff of 800 eV (for more details see text).

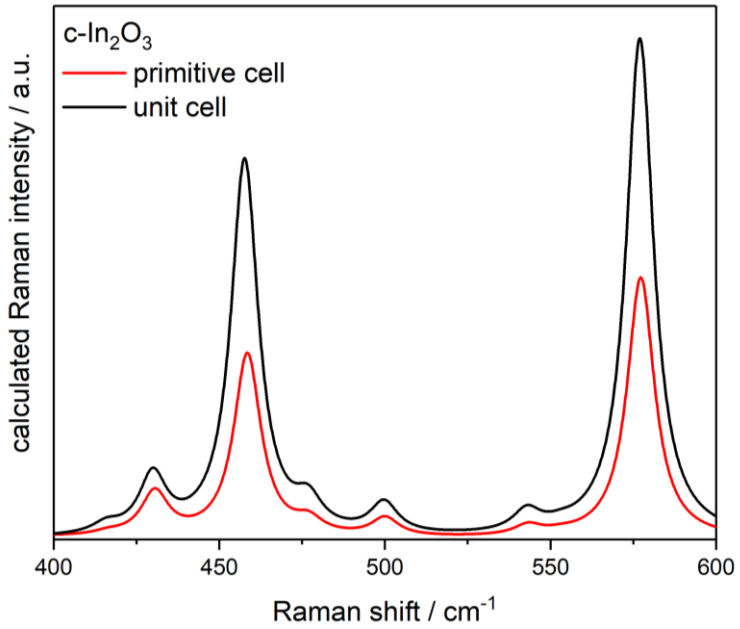

Figure S11: Comparison of a section of theoretical (DFT) Raman spectra of the non-defective primitive and unit In_2O_3 ($Ia\bar{3}$) cell.

References

(1) Brunauer, S.; Emmett, P. H.; Teller, E. Adsorption of Gases in Multimolecular Layers. *J. Am. Chem. Soc.* **1938**, *60* (2), 309–319. https://doi.org/10.1021/ja01269a023.

(2) Nottbohm, C. T.; Hess, C. Investigation of Ceria by Combined Raman, UV–Vis and X-Ray Photoelectron Spectroscopy. *Catal. Commun.* **2012**, *22*, 39–42. https://doi.org/10.1016/j.catcom.2012.02.009.

(3) Hess, C. Direct Correlation of the Dispersion and Structure in Vanadium Oxide Supported on Silica SBA-15. *J. Catal.* **2007**, *248* (1), 120–123. https://doi.org/10.1016/j.jcat.2007.02.024.

(4) Posada-Borbón, A.; Grönbeck, H. Hydrogen Adsorption on In_2O_3(111) and In_2O_3(110). *Phys. Chem. Chem. Phys.* **2020**, *22* (28), 16193–16202. https://doi.org/10.1039/D0CP01749C.

(5) Qi, Y.; Song, L.; Ouyang, S.; Liang, X.; Ning, S.; Zhang, Q.; Ye, J. Photoinduced Defect Engineering: Enhanced Photothermal Catalytic Performance of 2D Black In_2O_{3-x} Nanosheets with Bifunctional Oxygen Vacancies. *Adv. Mater.* **2020**, *32* (6), 1903915. https://doi.org/10.1002/adma.201903915.

(6) *Practical Surface Analysis by Auger and X-Ray Photoelectron Spectroscopy*; Briggs, D., Seah, M. P., Eds.; Wiley, 1983. https://doi.org/10.1016/0368-2048(84)80044-4.

(7) Nitsche, D.; Hess, C. In Situ Diagnostics of Catalytic Materials Using Tunable Confocal Raman Spectroscopy. *J. Raman Spectrosc.* **2013**, *44* (12), 1733–1738. https://doi.org/10.1002/jrs.4383.

(8) Waleska, P. S.; Hess, C. Oligomerization of Supported Vanadia: Structural Insight Using Surface-Science Models with Chemical Complexity. *J. Phys. Chem. C* **2016**, *120* (33), 18510–18519. https://doi.org/10.1021/acs.jpcc.6b01672.

(9) Schilling, C.; Hess, C. CO Oxidation on Ceria Supported Gold Catalysts Studied by Combined Operando Raman/UV–Vis and IR Spectroscopy. *Top. Catal.* **2017**, *60* (1–2), 131–140. https://doi.org/10.1007/s11244-016-0732-6.

(10) Schilling, C.; Ganduglia-Pirovano, M. V.; Hess, C. Experimental and Theoretical Study on the Nature of Adsorbed Oxygen Species on Shaped Ceria Nanoparticles. *J. Phys. Chem. Lett.* **2018**, *9* (22), 6593–6598. https://doi.org/10.1021/acs.jpclett.8b02728.

(11) Perdew, J. P.; Burke, K.; Ernzerhof, M. Generalized Gradient Approximation Made Simple. *Phys. Rev. Lett.* **1996**, *77* (18), 3865–3868. https://doi.org/10.1103/PhysRevLett.77.3865.

(12) Blöchl, P. E. Projector Augmented-Wave Method. *Phys. Rev. B* **1994**, *50* (24), 17953–17979. https://doi.org/10.1103/PhysRevB.50.17953.

(13) Monkhorst, H. J.; Pack, J. D. Special Points for Brillouin-Zone Integrations. *Phys. Rev. B* **1976**, *13* (12), 5188–5192. https://doi.org/10.1103/PhysRevB.13.5188.

(14) Schilling, C.; Hofmann, A.; Hess, C.; Ganduglia-Pirovano, M. V. Raman Spectra of Polycrystalline CeO_2: A Density Functional Theory Study. *J. Phys. Chem. C* **2017**, *121* (38), 20834–20849. https://doi.org/10.1021/acs.jpcc.7b06643.